Medbiotech Journal

MBTJ, 4(2): 83-86, 2020

Research Paper

Electrochemical Characterization of Titanium Oxide Nanoparticle through Anodic Oxidation

Alex Nemtsov [1], Pavel Kirshkov [2*]

[1] Department of Material Engineering, Agrikavosh Company, Nur-Sultan, Kazakhstan
[2] Department of Computational Chemistry, HiTech Institute for Theoretical and Computational Chemistry, India

Received: 05 April 2020 Accepted: 12 May 2020 Published: 01 June 2020

Abstract

Titanium oxide nanotubes were fabricated by anodic oxidation of a pure titanium sheet in 1.5 M H_2SO_4, 0.3 M H_3PO_4 and 0.3 M H_2O_2 mixture solution. The morphology of Titanium oxide nanotubes surface were investigated by scanning electron microscope (SEM). These tubes are well aligned and organized into high-density uniform arrays. While the tops of the tubes are open, the bottoms of the tubes are closed, forming a barrier layer structure similar to that of porous alumina. The average tube diameter, ranging in size from 40 to 70 nm.

Keywords: Nanotubes; Titanium Oxide; Anodizing; Scanning Electron Microscope

How to cite the article:
A. Nemtsov, P. Kirshkov, Electrochemical Characterization of Titanium Oxide Nanoparticle through Anodic Oxidation, Medbiotech J. 2020; 4(2): 83-86, DOI: 10.22034/MBT.2020.109583.

©2020 The Authors. This is an open access article under the CC By license

1. Introduction

Titanium and its alloys are increasingly used in technological applications due to their excellent mechanical properties, high corrosion resistance and good biocompatibility [1] . Furthermore oxide layers on Ti and particularly TiO_2 also have attracted much attention because TiO_2 possesses a variety of functional properties as for example for gas sensing, self-cleaning, solar energy conversion, wettability and photocatalysis applications [2-6] . In recent years, the formation of self-organized pores has been achieved on various valve metals Al, Zr, Hf, Nb, Ta and W including Ti [7-11] . In this work, we examine the morphology of porous titanium oxide thin films fabricated by anodizing pure titanium sheets under variable conditions. It has been found that the anodized titanium films have more complicated morphologies than anodized aluminum. In addition to porous films, such as those reported earlier well-aligned nanotube like structures composed of titanium oxide were obtained. In contrast to the continuous pore structures achieved with aluminum anodization, discrete titanium oxide nanotubes are found to grow from the discontinuous nanoporous titanium oxide film [9-14] .

*Corresponding author email: kirshkov@iitcc.org

2. Experimental

Pure titanium plates (purity %99.99, 25×10×1mm) were used. The chemical composition of samples has been given in table 1. The titanium specimens were mechanically polished and degreased in acetone for 5 min and then washed and dried. After the pre-treatment, Anodizing of titanium carried out with two methods:

a) Titanium Samples anodized in 0.5 wt% HF solution at a constant voltage of 20 V.

b) Titanium Samples anodized in 1.5M H_2SO_4+ 0.3M H_3PO_4+ 0.3M H_2O_2 mixture solution at a constant voltage of 70 V. The morphologies of the titanium oxide films were characterized with a Philips (Tokyo, Japan) scanning electron microscope (SEM).

Table 1. The chemical composition of Titanium used in this work

Element	Fe	O	Cu	Ni	C	Ti
Wt.%	0. 17	0. 29	0.07	0.09	0.04	rest

3. Results and Discussion

In anodizing process, titanium plates are immersed into an electrolyte and connected as an anode, leading to the formation of an oxide film at the surface. In moderately alkaline, neutral and moderately acidic aqueous solutions, TiO_2 is the only thermodynamically stable titanium compound, according to the Pourbaix diagram [12] . The corrosion potential of naked metallic titanium is more negative than that of water reduction, and thus rapid corrosion starts immediately upon immersion of titanium into any aqueous solution according to the equation $Ti + 2H_2O = TiO_2 + 2H_2$. TiO_2 layers are known to be very compact, poorly conducting, and only little permeable for water and gases, and furthermore the reversible potential of the oxidized surface (Ti/TiO_2 electrode) becomes more positive in comparison to the potential of the naked metal [13, 15, 16] . Consequently, the corrosion of titanium is a self-inhibiting process. The TiO_2 layer is highly resistive and the oxidation reaction will stop when the applied voltage is equal to the ohmic drop in the oxide film. Figure 1 shows current transient curves recorded during anodization in 0.5 wt% HF solution at a constant voltage of 20 V. For comparison the behavior in 1.5M H_2SO_4+0.3M H_3PO_4+0.3M H_2O_2 mixture solution at a constant voltage of 70 V is included. In the 0.5 wt% HF containing electrolyte a clear deviation from the behavior in the 1.5M H_2SO_4+0.3M H_3PO_4+0.3M H_2O_2 mixture electrolyte can be observed, that is, on the one hand that the current drops more slowly in the initial phase and on the other hand the current rises again after the initial decay. After extended polarization the current density in HF containing electrolyte is higher than the steady-state in 1.5M H_2SO_4+0.3M H_3PO_4+0.3M H_2O_2 mixture electrolyte, which indicates that an additional dissolution process takes place in the presence of fluorides. This finding can be ascribed to the dissolution of the electrochemically formed TiO_2 as soluble hexafluorotitanium complexes $[TiF_6]^{-2}$, which go into solution. The curve shape, showing a decrease/ increase/decrease sequence, has been reported on Al and Ti, and may be assigned to different stages during a self-ordering process [17, 18] . In 1.5M H_2SO_4+0.3M H_3PO_4+0.3M H_2O_2 mixture electrolyte, on the other hand, extended anodization resulted in a steady-state value that represents a leakage through a compact oxide layer. After anodization in this electrolyte no porous structures could be observed – just a compact oxide layer was present on the surface.

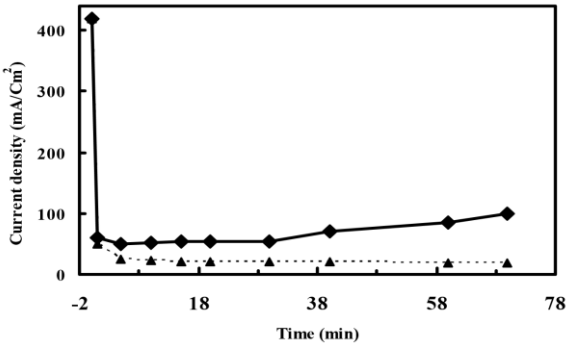

Figure 1. Current transient curves during electrochemical anodization in 0.5 wt% HF solution (solid line) and in 1.5M H_2SO_4+0.3M H_3PO_4+0.3M H_2O_2 mixture solution (dashed line).

SEM permits observation of specimens with large magnification and great depth of field by means of detection of secondary electrons. The number of secondary electrons depends on several factors, the most important being the angle between the primary electron beam and the local surface of the observed specimen. Figure 2(a) shows a typical scanning electron microscope (SEM) micrograph of the porous structures obtained under anodizing voltage 70 V, in 1.5 M H_2SO_4, 0.3 M H_3PO_4 and 0.3 M H_2O_2 mixture. The morphology of the porous film is similar to that of porous (sponge like) alumina, with a typical pore size of 40 to 70 nm. It can be seen that Titanium oxide nanotubes exhibits uniform tube morphology, the tubes open on the top and close at the bottom, nearly parallel and closed side by side. Figure 2(b) shows a SEM image of the porous structures obtained under anodizing voltage 20 V, in 0.5 wt% HF solution. It is clear that the anodic TiO_2 layer was less porous than that of anodic film

formed in 1.5M H_2SO_4+0.3M H_3PO_4+0.3M H_2O_2 mixture. The SEM images show that the Surface morphologies of anodic TiO_2 films, depends on electrolyte composition and working conditions in anodizing [5, 19, 20] .

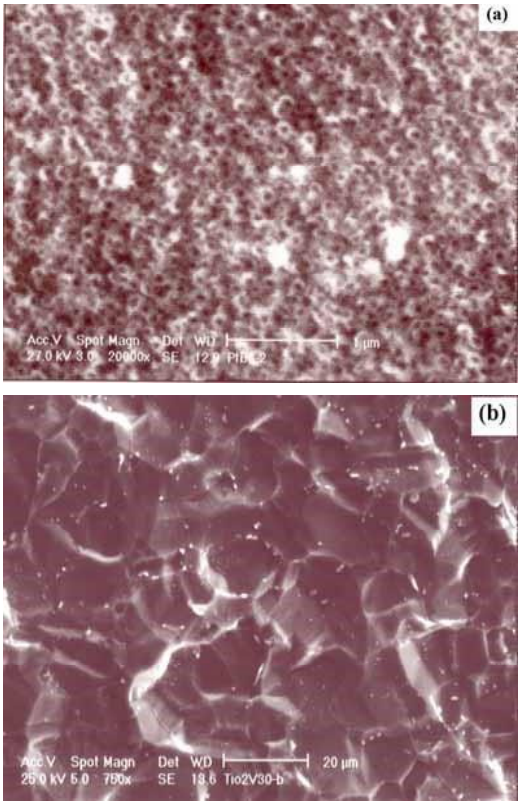

Figure 2. Surface morphologies of (a) Titanium sheet anodized under voltage of 70 V in 1.5 M H2SO4 + 0.3 M H3PO4 + 0.3 M H2O2 mixture solution (b) Titanium sheet anodized under voltage of 20 V in 0.5 wt% HF solution.

4. Conclusions

well-aligned titanium oxide nanotubelike arrays have been obtained through titanium anodization in 1.5M H_2SO_4+ 0.3M H_3PO_4+ 0.3M H_2O_2 mixture solution at a constant voltage of 70 V. The resulting nanotubes are straight, with a pore size ranging from 40 to 70 nm, and have a barrier layer at their bottom. The SEM images show that the Surface morphologies of anodic TiO_2 films, depends on electrolyte composition and working conditions in anodizing.

References

1. Le Goff A, Gorgy K, Holzinger M, Haddad R, Zimmerman M, Cosnier S. 2011. Tris(bispyrene-bipyridine)iron(II): A Supramolecular Bridge for the Biofunctionalization of Carbon Nanotubes via π-Stacking and Pyrene/β-Cyclodextrin Host–Guest Interactions. *Chemistry – A European Journal* 17(37): 10216-10221.

2. Ferreira GMD, Ferreira GMD, Almeida GWR, Soares NFF, Pires ACS, Silva LHM. 2019. Thermodynamics of multi-walled carbon nanotube biofunctionalization using nisin: The effect of peptide structure. *Colloids and Surfaces A: Physicochemical and Engineering Aspects* 578: 123611.

3. Paul KB, Singh V, Vanjari SRK, Singh SG. 2017. One step biofunctionalized electrospun multiwalled carbon nanotubes embedded zinc oxide nanowire interface for highly sensitive detection of carcinoma antigen-125. *Biosensors and Bioelectronics* 88: 144-152.

4. Haddad R, Cosnier S, Maaref A, Holzinger M. 2009. Non-covalent biofunctionalization of single-walled carbon nanotubesviabiotin attachment by π-stacking interactions and pyrrole polymerization. *Analyst* 134(12): 2412-2418.

5. Safoora Eissazadeh MHJ, Sara Kashisaz, Mohsen Manna. 2019. Investigation into the Bending Performance of Steel Beams Reinforced with Carbon Fiber Polymer Under Nonlinear Analysis. *Journal of Computational and Theoretical Nanoscience* 16(01): 269-274.

6. Eissazadeh S, Jafari MH, Kashisaz S, Manna M. 2019. Investigation into the Bending Performance of Steel Beams Reinforced with Carbon Fiber Polymer Under Nonlinear Analysis. *Journal of Computational and Theoretical Nanoscience* 16(1): 269-274.

7. Safoora Eissazadeh MHJ, Sara Kashisaz, Mohsen Manna. 2019. Investigation into the Behavior of Square Concrete-Reinforced Columns Under Axial Loading, Retrofitted by Fiber-Reinforced Polymer and Steel Jacket. *Journal of Computational and Theoretical Nanoscience* 16(01): 295-307.

8. Eissazadeh S, Jafari MH, Kashisaz S, Manna M. 2019. Investigation into the Behavior of Square Concrete-Reinforced Columns Under Axial Loading, Retrofitted by Fiber-Reinforced Polymer and Steel Jacket. *Journal of Computational and Theoretical Nanoscience* 16(1): 295-307.

9. Shamsin Beyranvand H, Mirzaei Ghaleh Ghobadi M, Sarlak H. 2020. Experimental Study of Carbon Dioxide Absorption in Diethyl Ethanolamine (DEEA) in the Presence of Titanium Dioxide (TiO2). *Progress in Chemical and Biochemical Research* 3(1): 55-63. en.

10. Kumagai M, Sarma TK, Cabral H, Kaida S, Sekino M, Herlambang N, et al. 2010. Enhanced in vivo Magnetic Resonance Imaging of Tumors by PEGylated Iron-Oxide–Gold Core–Shell Nanoparticles with Prolonged Blood Circulation Properties. *Macromolecular Rapid Communications* 31(17): 1521-1528.

11. Jafari MH, Kashisaz S, Manna M. 2019. Effects of Nanoparticles on the Durability and Mechanical Properties of Concrete. *Journal of Computational and Theoretical Nanoscience* 16(1): 275-283.

12. Esmaeilimotlagh M, Basiri Z, Kheirabadi MA, Oveisi K. 2019. The Effect of Information and Communication Technology on the Professional Development of Teachers. *Journal of Computational and Theoretical Nanoscience* 16(1): 312-318.
13. Yaghoubi Nezhad A, Soltantabar Shahabedini A, Ali H. 2020. Determination of small amounts of fluoxetine in a biological sample through solid phase extraction method by carbon nanotubes. *Eurasian Chemical Communications*. en.
14. Kheirabadi MA, Jafari MH, Alizadeh F, Basiri Z, Oveisi K. 2019. Comparison and Satisfaction of Injured Management System for Students Athlete in the Sport Federations. *Journal of Computational and Theoretical Nanoscience* 16(1): 284-288.
15. Hwang J-Y, Shin US, Jang W-C, Hyun JK, Wall IB, Kim H-W. 2013. Biofunctionalized carbon nanotubes in neural regeneration: a mini-review. *Nanoscale* 5(2): 487-497.
16. Jalali-Heravi M, Parastar H, Ebrahimi-Najafabadi H. 2009. Characterization of volatile components of Iranian saffron using factorial-based response surface modeling of ultrasonic extraction combined with gas chromatography–mass spectrometry analysis. *Journal of Chromatography A* 1216(33): 6088-6097.
17. Ibrahim HM, Yusoff WMW, Hamid AA, Illias RM, Hassan O, Omar O. 2005. Optimization of medium for the production of β-cyclodextrin glucanotransferase using Central Composite Design (CCD). *Process Biochemistry* 40(2): 753-758.
18. Ogbuagu AS-M, Okoye CI. 2020. Physico-chemical characterization of Avocado (Persea americana Mill.) Oil from Tree Indonesian Avocado Cultivars. *Progress in Chemical and Biochemical Research* 3(1): 39-45. en.
19. Aadesariya MK, Ram VR, Dave PN. 2019. Investigation of phytochemicals in methanolic leaves extracts of Abutilon pannosum and Grewia tenax by Q-TOF LC/MS. *Progress in Chemical and Biochemical Research* 2(1): 13-19. en.
20. Kashisaz S, Basiri Paknafs Z, Riahi A. 2020. The Milling of Metalsthrough Adaptive Neuro-FuzzyInference System (ANFIS) for non-touch Measuring of the Temperature to Reduce Coolant. *Journal of Modern Processes in Manufacturing and Production* 9(2): 23-30.